Electronic Supplementary Information

Homodiamine-Functionalized Metal-Organic Frameworks with MOF-74-Type Extended Structure for Superior Selectivity of CO_2 over N_2

Je Seon Yeon,[a] Woo Ram Lee,[a] Nam Woo Kim,[a] Hyuna Jo,[a] Hanyeong Lee,[b] Jeong Hwa Song,[a] Kwang Soo Lim,[a] Dong Won Kang,[a] Jeong Gil Seo,[b] Dohyun Moon,[c] Brian Wiers,[d] and Chang Seop Hong*[a]

a. Department of Chemistry, Korea University, 136-713 Seoul, Republic of Korea.

b. Department of Energy and Biotechnology, Myongji University, 449-728 Yongin, Gyeonggi-do, Republic of Korea.

c. Beamline Division, Pohang Accelerator Laboratory, 790-784 Pohang, Kyungbuk, Republic of Korea.

d. Department of Chemistry, University of California, Berkeley, 94720 California, United States.

*To whom correspondence should be addressed.

Tel.: +82 232903138. E-mail: cshong@korea.ac.kr (Chang Seop Hong)

Powder X-ray Diffraction and Structure Modeling. PXRD data were recorded using Cu Kα (λ = 1.5406 Å) on a Rigaku Ultima III diffractometer with a scan speed of 2°/min and a step size of 0.01° . The synchrotron powder X-ray diffraction data were collected at 298K with the 240 mm of detector distance in 2400 s exposure with synchrotron radiation (λ = 1.09998Å) using a 2D SMC ADSC Quantum-210 detector with a silicon (111) double crystal monochromator at the Pohang Accelerator Laboratory. The ADX program[1] was used for data collection, and Fit2D program[2] was used for converting a two-dimensional diffraction image to a one-dimensional diffraction pattern. The unit cell dimension of **1** was determined by conducting a full-pattern decomposition with the Le Bail method (Pawley refinement) implemented in *TOPAS-Academic*. The trigonal space group $P3_221$ was utilized for the refinements, due to the isomorphism with Zn_2(dobpdc).[3] Based on the unit cell dimensions obtained, the geometry of the backbones was optimized via an energy minimization algorithm using the universal force field implemented in the *Forcite* module of *Materials Studio*.[4]

Gas Sorption Measurements. Gas sorption isotherms were measured using a Micromeritics ASAP2020 instrument up to 1 atm of gas pressure unless otherwise stated. The highly pure N_2 (99.999%) and CO_2 (99.999%) were used in the sorption experiments. N_2 gas isotherms were measured at 77 K and 298 K, and CO_2 uptake was measured at 298 K, 313 K, and 333 K.

Thermogravimetric Analyses and Gas Cycling Measurements. Thermogravimetric analyses (TGA) were carried out at a ramp rate of 2 °C/min in an Ar (99.999 %) flow using a Scinco TGA N-1000 instrument. CO_2 cycling experiments of the activated **1** were carried out on the instrument with 15% CO_2 in N_2 and Ar (99.999 %). A flow rate of 60 mL/min was applied for all gases. We conducted cycling experiments using fresh samples of **1-en**, **1-mmen**, and **1-ppz**.

Infrared Spectroscopy Measurements. Infrared spectra were obtained with KBr pellets and an air-tight homemade IR cell composed of NaCl windows using a Thermo Nicollet 380 spectrometer. Prior to the IR measurements, N_2 was purged into a sample chamber, a detector, and an IR source to remove CO_2 in air. Variable temperature infrared spectra were collected with a homemade IR cell sandwiched by two CaF_2 windows using a Varian 640-IR spectrometer. For this experiment, N_2 was purged into a sample chamber.

Other Physical Measurement. Elemental analyses for C, H, and N were performed at the Elemental Analysis Service Center of Sogang University.

[Reference]

1. A. J. Arvai, C. Nielsen, ADSC Quantum-210 ADX Program, Area Detector System Corporation; Poway, CA, USA, 1983.
2. Fit2D Program: Hammersley, A. (E-mail: hammersley@esrf.fr), ESRF, 6 RUE JULES HOROWITZ BP 220 38043 GRENOBLE CEDEX 9 FRANCE.
3. T. M. McDonald, W. R. Lee, J. A. Mason, B. M. Wiers, C. S. Hong, J. R. Long, *J. Am. Chem. Soc.* **2012**, *134*, 7056-7065.
4. H. Deng, S. Grunder, K. E. Cordova, C. Valente, H. Furukawa, M. Hmadeh, F. Gandara, A. C. Whalley, Z. Liu, S. Asahina, H. Kazumori, M. O'Keeffe, O. Terasaki, J. F. Stoddart, O. M. Yaghi, *Science* **2012**, *336*, 1018-1023.

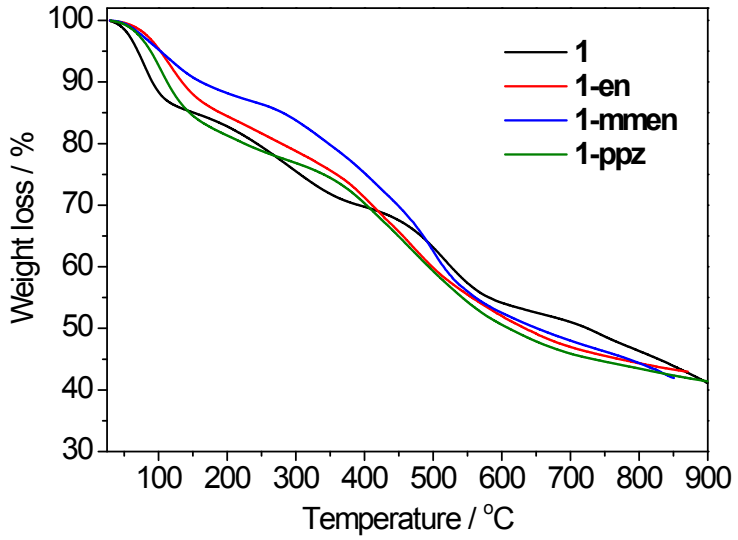

Fig. S1 TGA curves of **1**, **1-en**, **1-mmen**, and **1-ppz**.

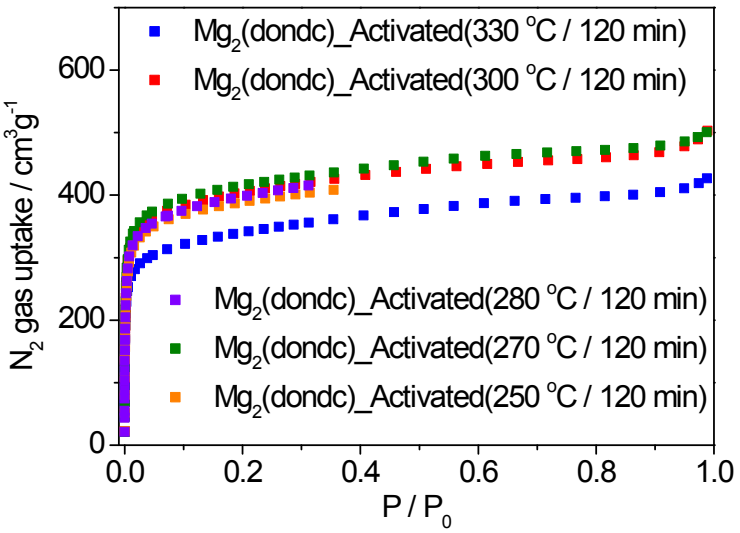

Fig. S2 N_2 adsorption isotherms for **1** at 77 K after evacuuation at 250 °C, 270 °C, 280 °C, 300 °C, and 330 °C for 120 min.

Table S1 Dual-Site Langmuir-Freundlich parameters for the pre-step region of the CO_2 adsorption isotherm for **1** at 25 °C, 40 °C and 60 °C.

	25°C	**40°C**	**60°C**
$q_{sat,\,A}$ / mmol g^{-1}	4.55211	4.66138	4.42028
b_A / bar^{-a}	0.12351	0.05442	8.07059E-4
α_A	0.94695	0.93942	0.82142
$q_{sat,\,B}$ / mmol g^{-1}	354.79891	195.5888	4.50301
b_B / bar^{-a}	3.88037E-5	3.66082E-5	0.02182
α_B	0.71665	0.76074	0.94873

Table S2 Dual-Site Langmuir-Freundlich parameters for the pre-step region of the CO_2 adsorption isotherm for **1-en** at 25 °C, 40 °C and 60 °C.

	25°C	**40°C**	**60°C**
$q_{sat,\,A}$ / mmol g^{-1}	762.86421	1.46813	1.76253
b_A / bar^{-a}	2.51115E-5	0.35548	0.18625
α_A	0.57065	1.15327	0.68145
$q_{sat,\,B}$ / mmol g^{-1}	1.63988	12.7984	152.43367
b_B / bar^{-a}	0.4778	0.00271	1.33762E-5
α_B	1.26149	0.4909	0.78779

Table S3 Dual-Site Langmuir-Freundlich parameters for the pre-step region of the CO_2 adsorption isotherm for **1-mmen** at 25 °C, 40 °C and 60 °C.

	20°C	**40°C**	**60°C**
$q_{sat,\,A}$ / mmol g^{-1}	0.02233	0.05694	0.06354
b_A / bar^{-a}	1	6.77	0.5
α_A	1	0.99	1
$q_{sat,\,B}$ / mmol g^{-1}	2.9	0.5	1.5
b_B / bar^{-a}	0.241	0.53	0.3
α_B	1	1	1

Table S4 Modified dual-Site Langmuir-Freundlich parameters for the post-step region of the CO_2 adsorption isotherm for **1-mmen** at 25 °C, 40 °C and 60 °C.

	25°C	**40°C**	**60°C**
P_{step}	0.07792	0.09255	0.05336
$q_{sat,\,A}$ / mmol g^{-1}	4.1	2.70493	0.46966
b_A / bar^{-a}	2.32603E-20	0.10535	2.0734
α_A	0.98406	1	1
$q_{sat,\,B}$ / mmol $^{g-1}$	8.62966	6.76199	0.60374
b_B / bar^{-a}	0.00227	1.02088E-4	0.05258
α_B	0.71611	1	0.89334
$q_{sat,\,C}$ / mmol $^{g-1}$	6.54443	0.71149	0.83103
b_C / bar^{-a}	0.2285	5.60173	0.06285
α_C	0.55075	0.88648	1

Table S5 Dual-Site Langmuir-Freundlich parameters for the pre-step region of the CO_2 adsorption isotherm for **1-ppz** at 25 °C, 40 °C and 60 °C.

	25°C	**40°C**	**60°C**
$q_{sat,\ A}$ / mmol g^{-1}	6681.99525	483294	1.42901
b_A / bar^{-a}	1.21065E-6	0.01198	0.10514
α_A	0.72298	0.4687	1.13155
$q_{sat,\ B}$ / mmol g^{-1}	1.64314	1.16535	8.00513
b_B / bar^{-a}	0.48951	0.22381	0.00252
α_B	1.5	1.67732	0.52483

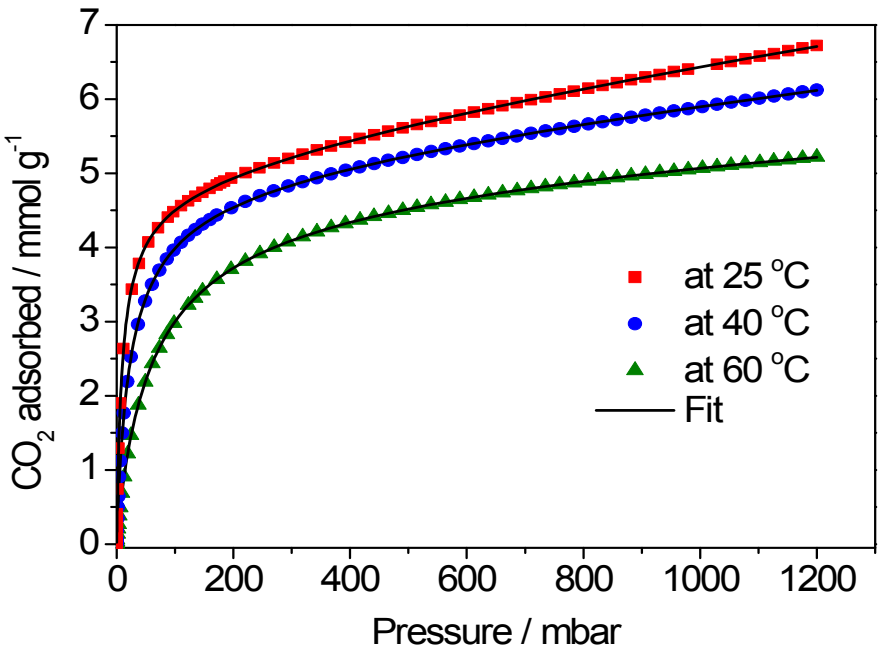

Fig. S3 CO_2 isotherms and fits based on a dual-site Langmuir-Freundlich equation for **1** at 25 °C, 40 °C and 60°C.

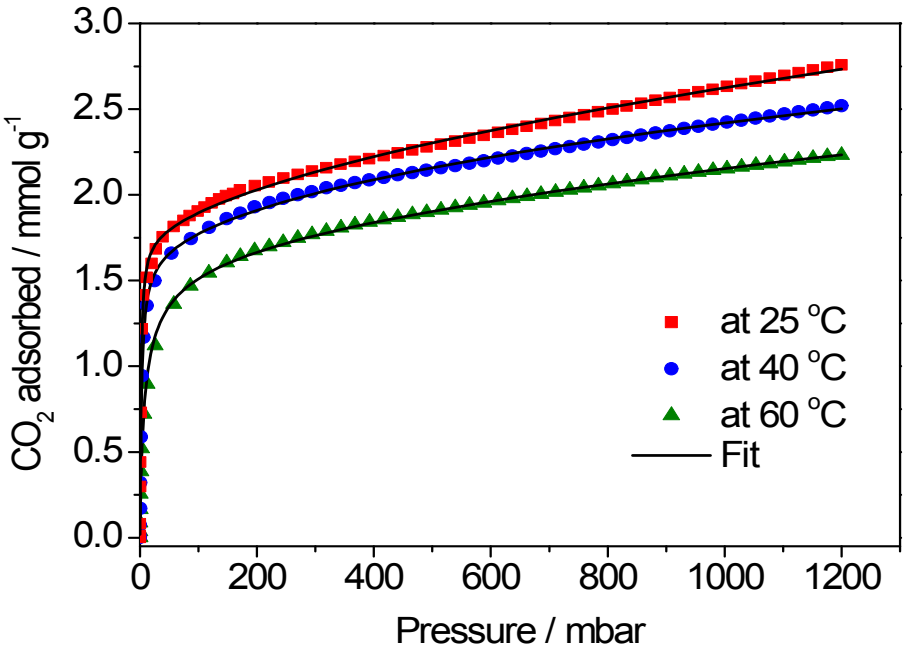

Fig. S4 CO_2 isotherms and fits based on a dual-site Langmuir-Freundlich equation for **1-en** at 25 °C, 40 °C and 60°C

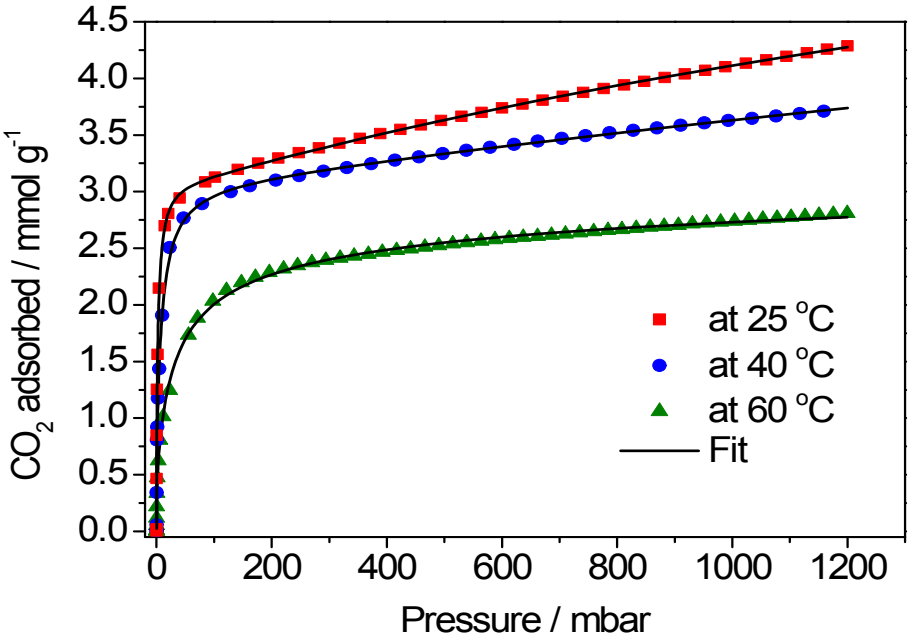

Fig. S5. CO_2 isotherms and fits based on a dual-site Langmuir-Freundlich equation for **1-mmen** at 25 °C, 40 °C and 60°C

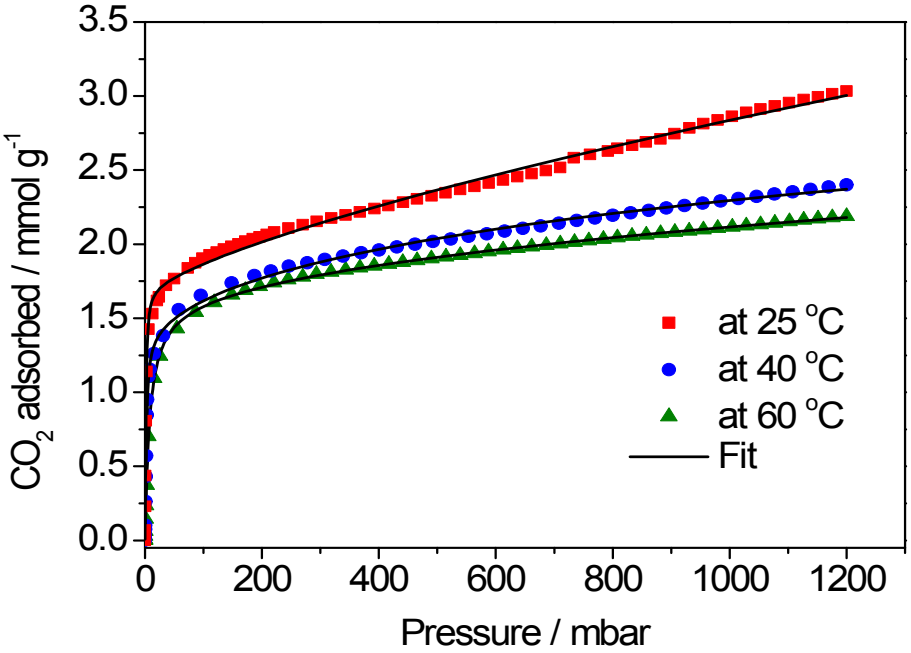

Fig. S6. CO_2 isotherms and fits based on a dual-site Langmuir-Freundlich equation for **1-ppz** at 25 °C, 40 °C and 60°C

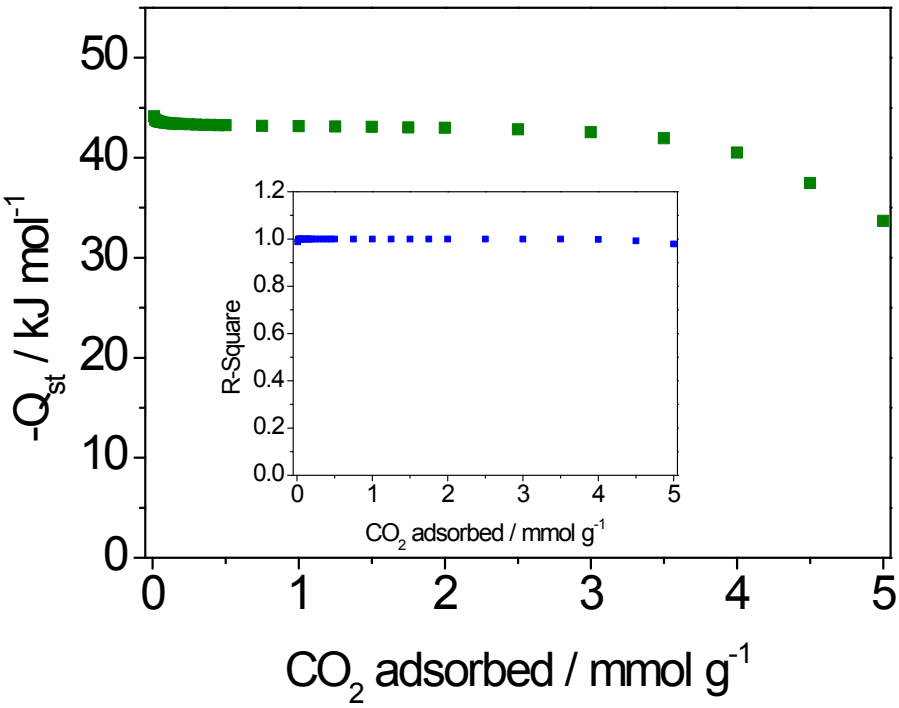

Fig. S7 Isosteric heats of adsorption ($-Q_{st}$) as a function of loading for CO_2 in **1**. Inset: Residual sum of squares (R^2) for the best fit line of ln$p$ versus $1/T$ as a function of the constant CO_2 loading used in the Clausius-Clapeyron equation.

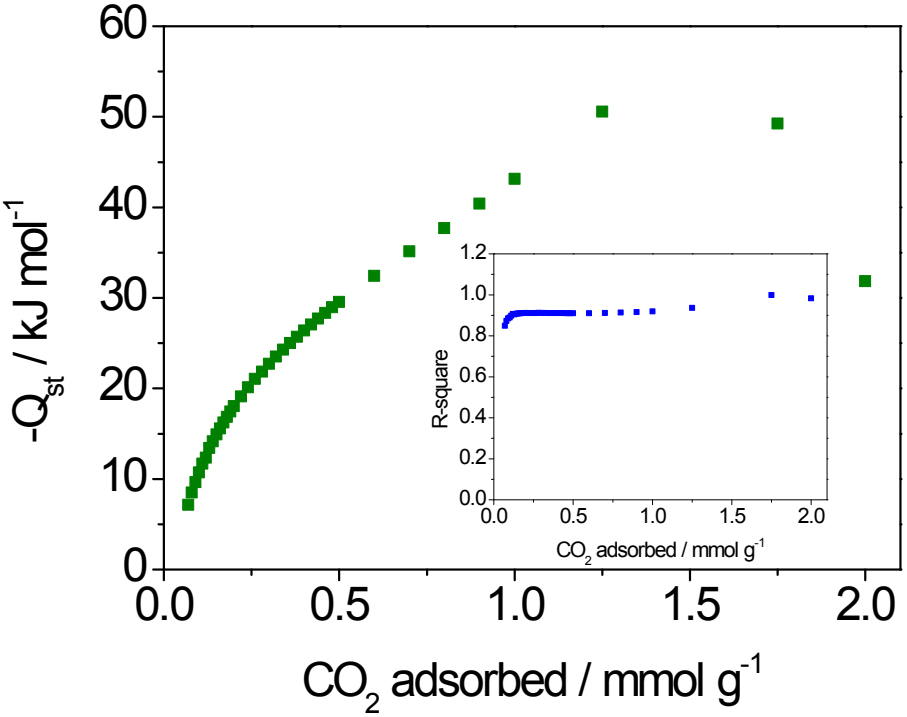

Fig. S8 Isosteric heats of adsorption ($-Q_{st}$) as a function of loading for CO_2 in **1-en**. Inset: Residual sum of squares (R^2) for the best fit line of ln$p$ versus $1/T$ as a function of the constant CO_2 loading used in the Clausius-Clapeyron equation.

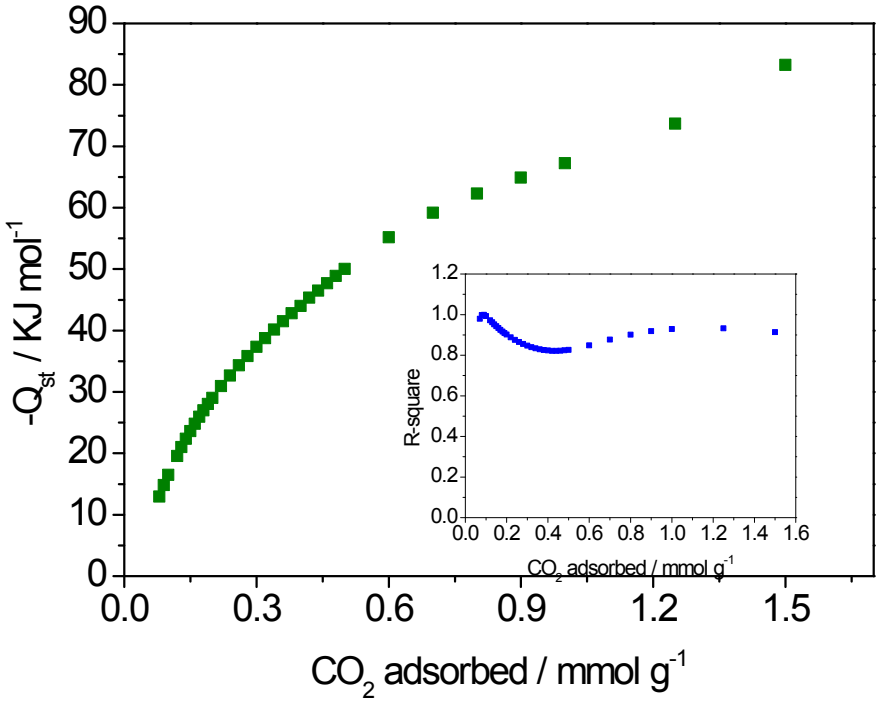

Fig. S9 Isosteric heats of adsorption ($-Q_{st}$) as a function of loading for CO_2 in **1-mmen**. Inset: Residual sum of squares (R^2) for the best fit line of ln$p$ versus $1/T$ as a function of the constant CO_2 loading used in the Clausius-Clapeyron equation.

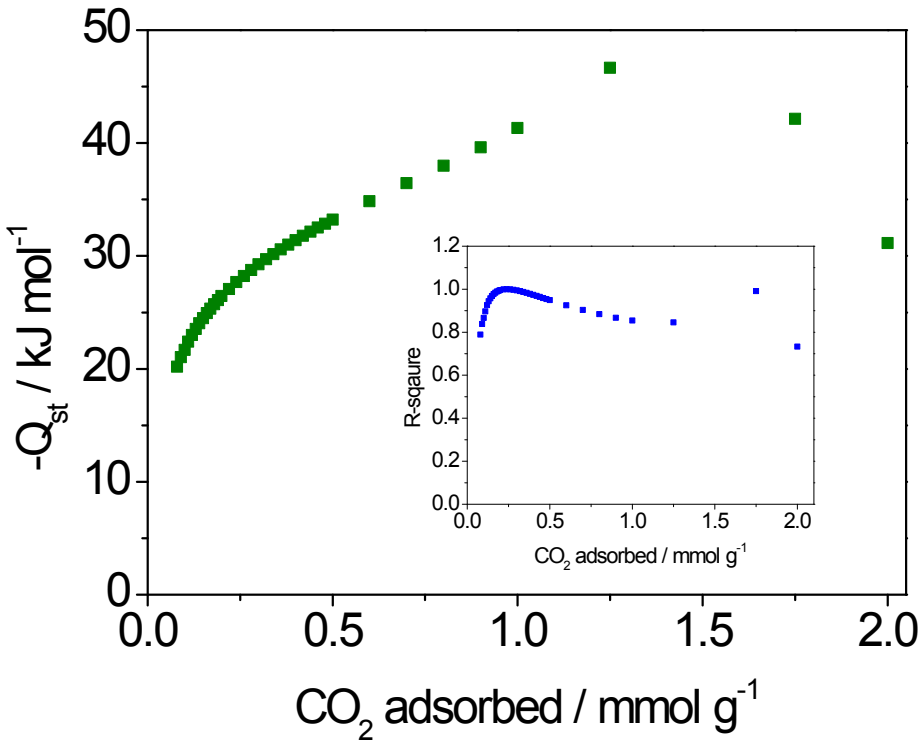

Fig. S10 Isosteric heats of adsorption ($-Q_{st}$) as a function of loading for CO_2 in **1-ppz**. Inset: Residual sum of squares (R^2) for the best fit line of ln$p$ versus $1/T$ as a function of the constant CO_2 loading used in the Clausius-Clapeyron equation.

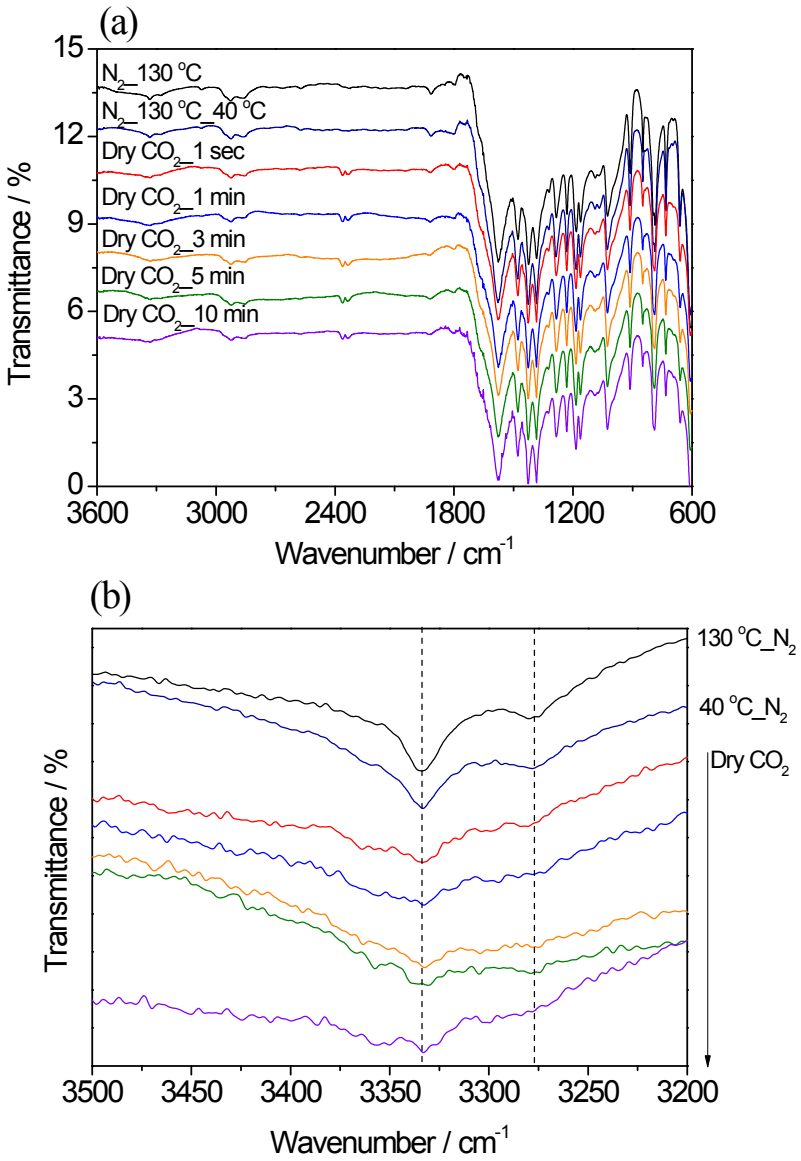

Fig. S11 (a) In-situ IR data of **1-en**. The cell was heated at 130 ºC and then cooled down to 40 ºC under N_2 flowing. A stream of 15% CO_2 balanced with N_2 was infused into the cell and in-situ IR data were collected at different times. (b) Enlargement of the IR spectra in the high frequency range.

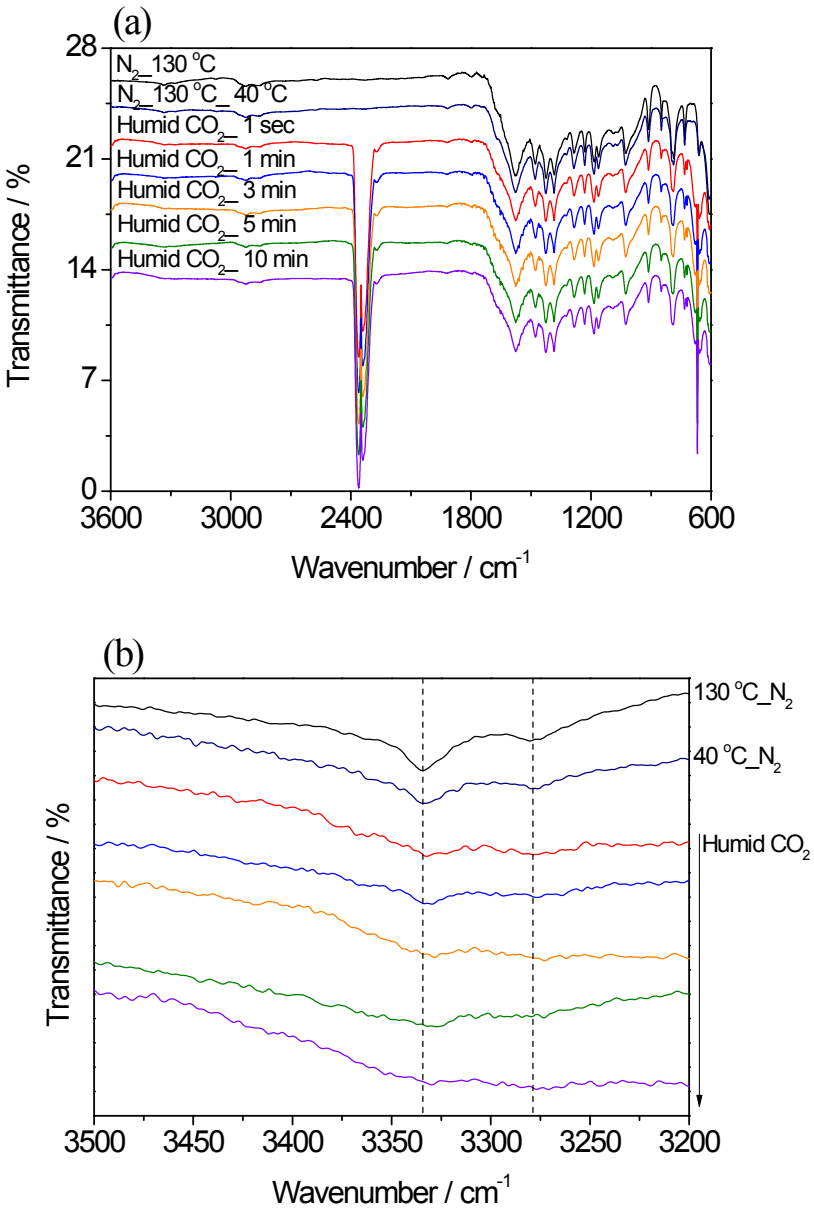

Fig. S12 (a) In-situ IR data of **1-en**. The cell was heated at 130 ºC and then cooled down to 40 ºC under N_2 flowing. Humid 15% CO_2 was infused into the cell and in-situ IR data were collected at different times. (b) Enlargement of the IR spectra in the high frequency range.

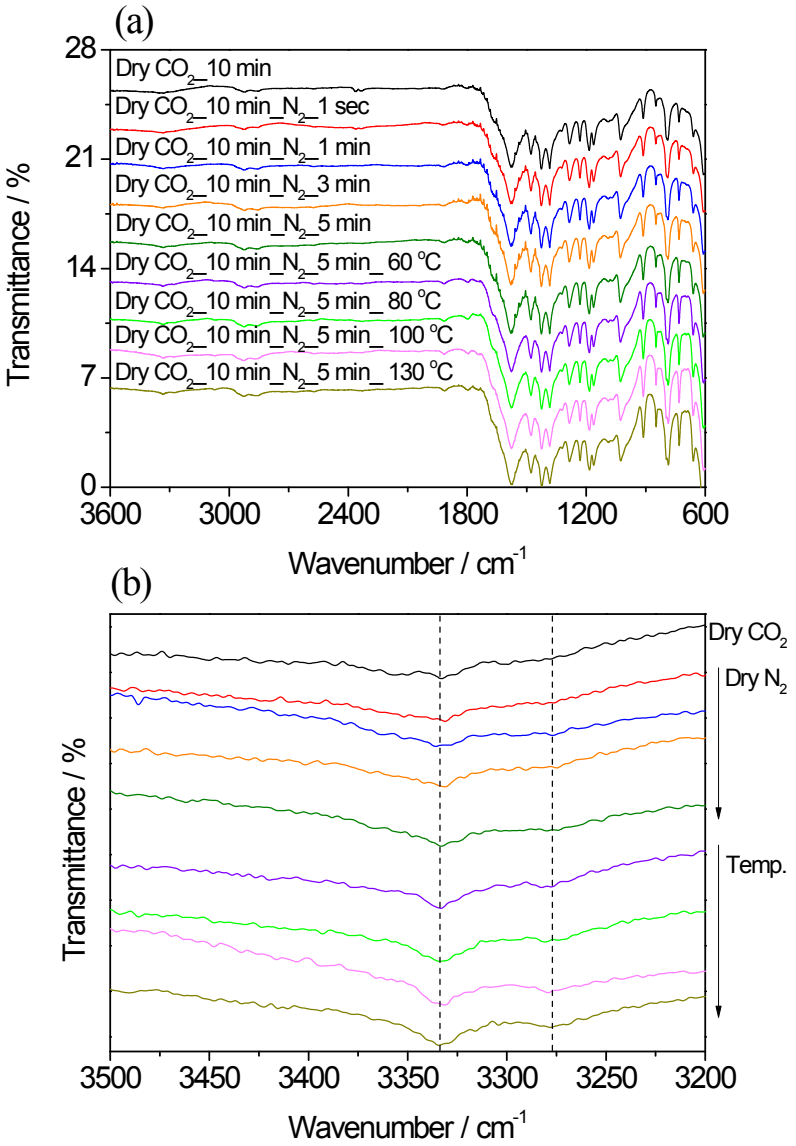

Fig. S13 (a) In-situ IR data of **1-en**. CO_2 (15%) was flowed into the cell for 10 min and then N_2 was infused into it for different times. The temperature was increased from 40 °C to 130 °C. (b) Enlargement of the IR spectra in the high frequency range.

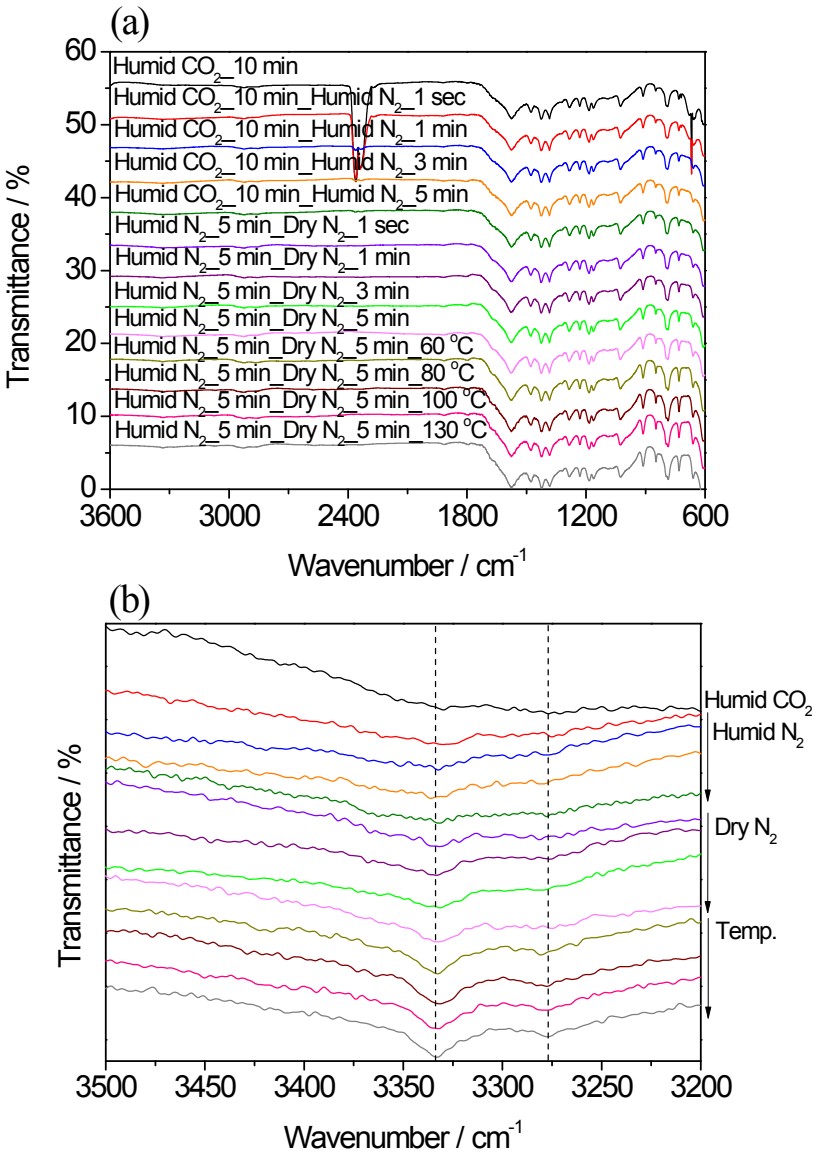

Fig. S14 (a) In-situ IR data of **1-en**. Humid CO_2 (15%) was flowed into the cell for 10 min and then N_2 was infused into it for different times. The temperature was increased from 40 °C to 130 °C. (b) Enlargement of the IR spectra in the high frequency range.

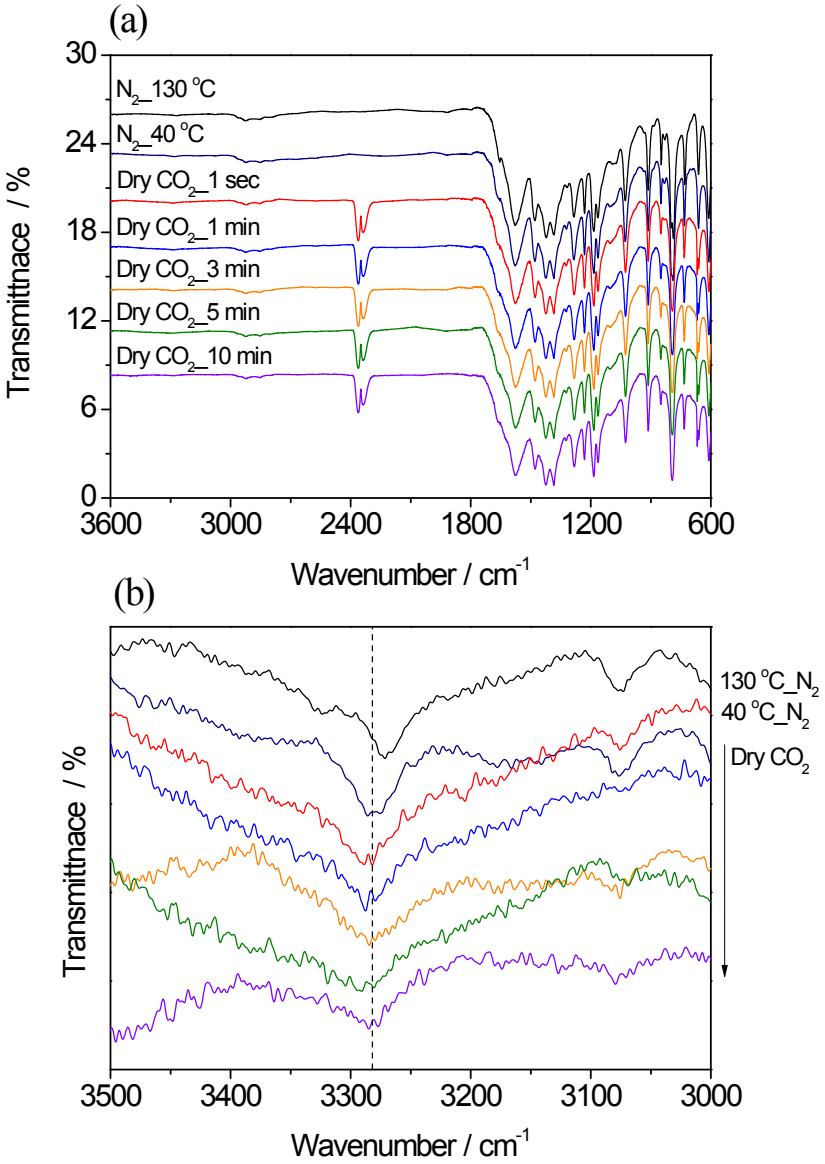

Fig. S15 (a) In-situ IR data of **1-mmen**. The cell was heated at 130 °C and then cooled down to 40 °C under N_2 flowing. A stream of 15% CO_2 balanced with N_2 was infused into the cell and in-situ IR data were collected at different times. (b) Enlargement of the IR spectra in the high frequency range.

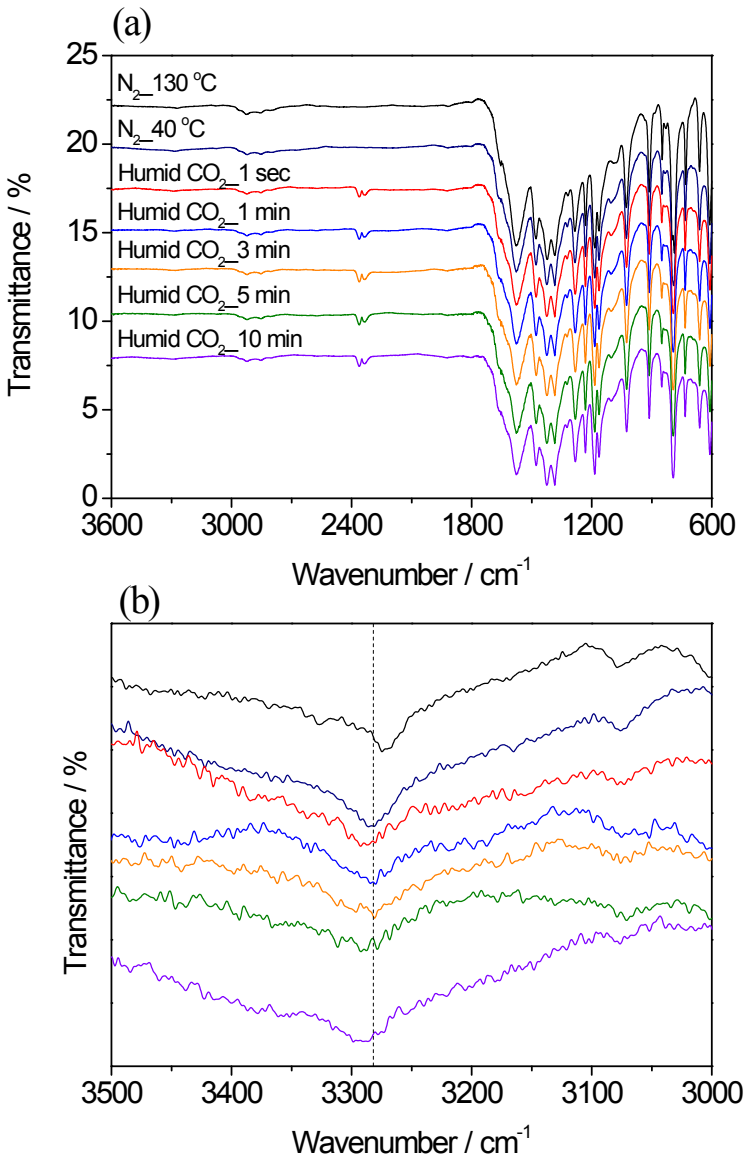

Fig. S16 (a) In-situ IR data of **1-mmen**. The cell was heated at 130 °C and then cooled down to 40 °C under N_2 flowing. Humid 15% CO_2 was infused into the cell and in-situ IR data were collected at different times. (b) Enlargement of the IR spectra in the high frequency range.

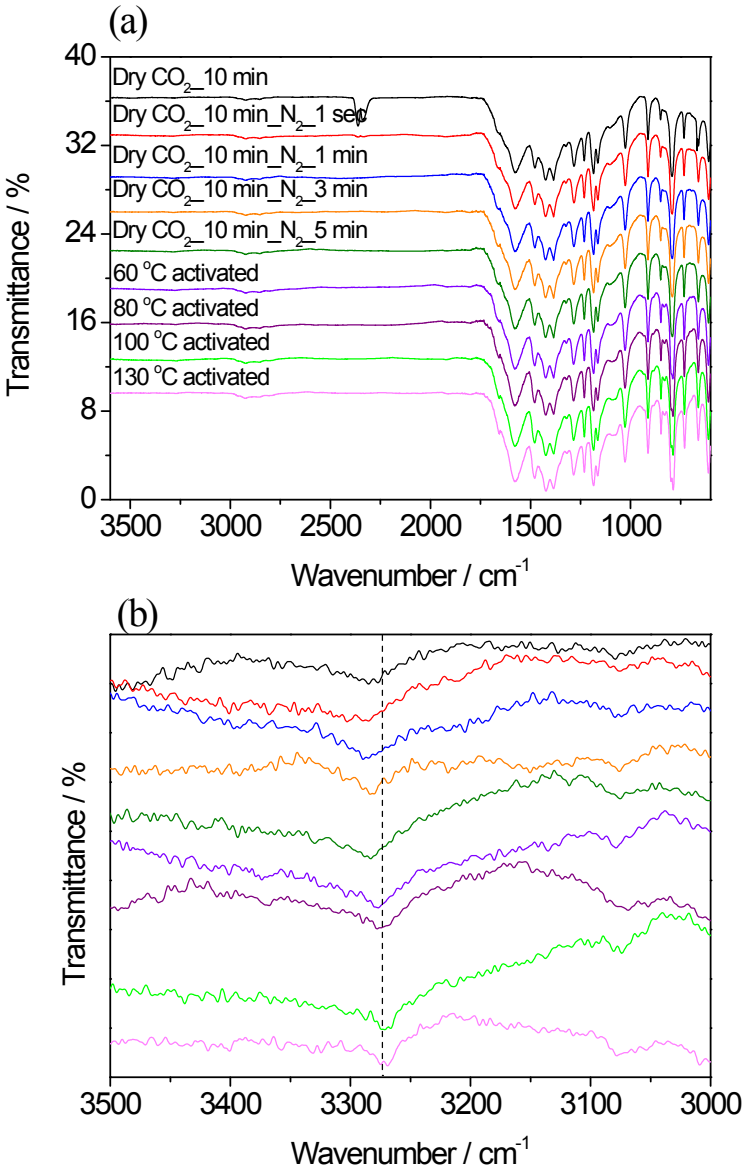

Fig. S17 (a) In-situ IR data of **1-mmen**. CO_2 (15%) was flowed into the cell for 10 min and then N_2 was infused into it for different times. The temperature was increased from 40 °C to 130 °C. (b) Enlargement of the IR spectra in the high frequency range.

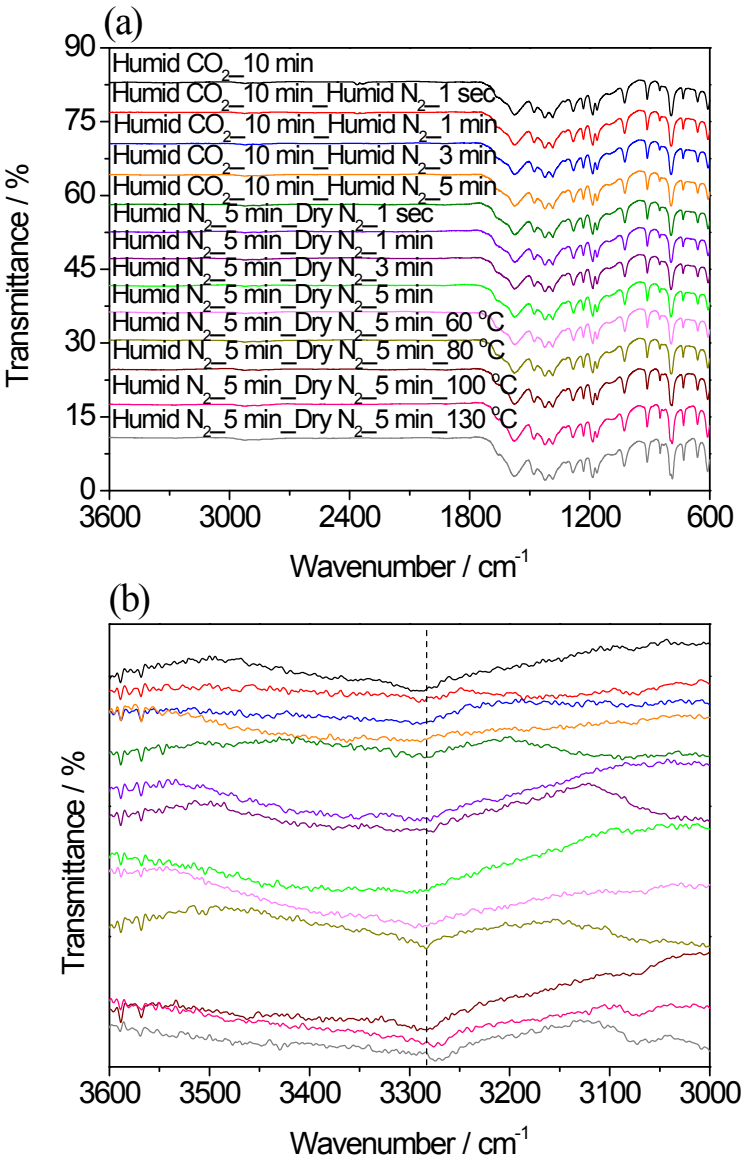

Fig. S18 (a) In-situ IR data of **1-mmen**. Humid CO_2 (15%) was flowed into the cell for 10 min and then N_2 was infused into it for different times. The temperature was increased from 40 °C to 130 °C. (b) Enlargement of the IR spectra in the high frequency range.

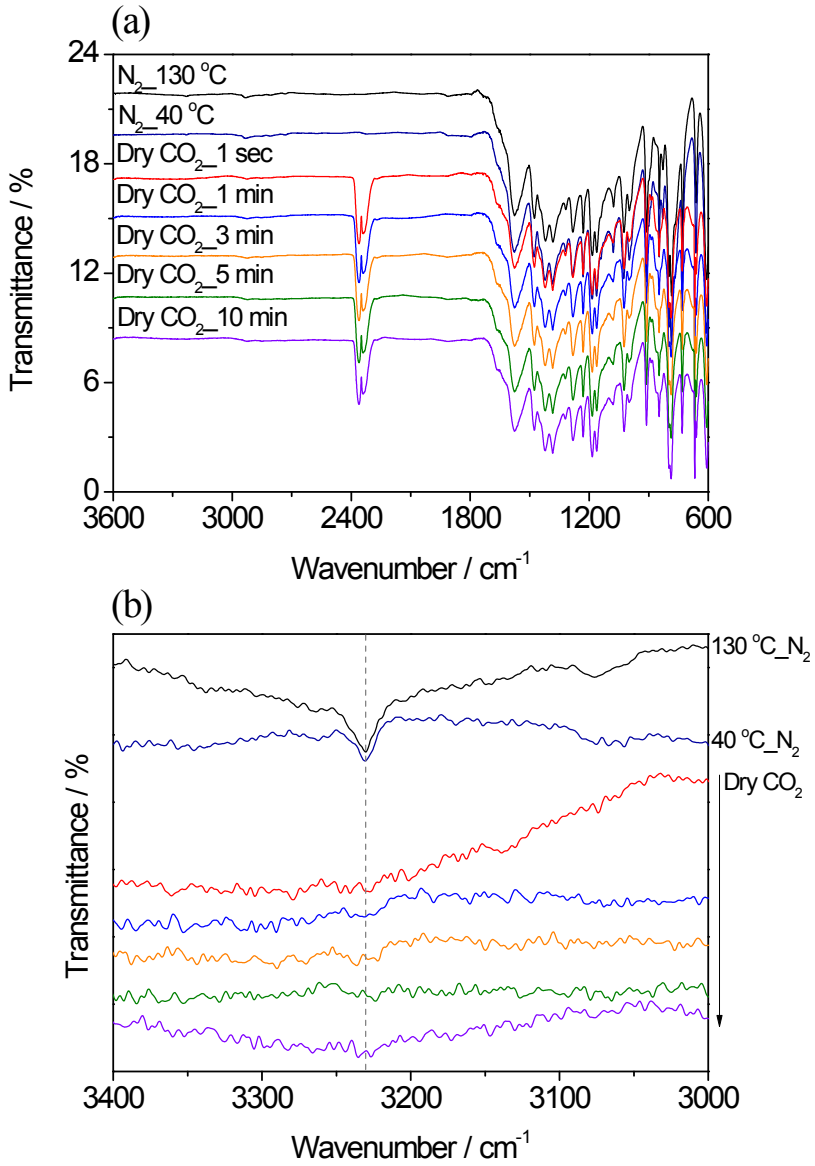

Fig. S19 (a) In-situ IR data of **1-ppz**. The cell was heated at 130 °C and then cooled down to 40 °C under N_2 flowing. A stream of 15% CO_2 balanced with N_2 was infused into the cell and in-situ IR data were collected at different times. (b) Enlargement of the IR spectra in the high frequency range.

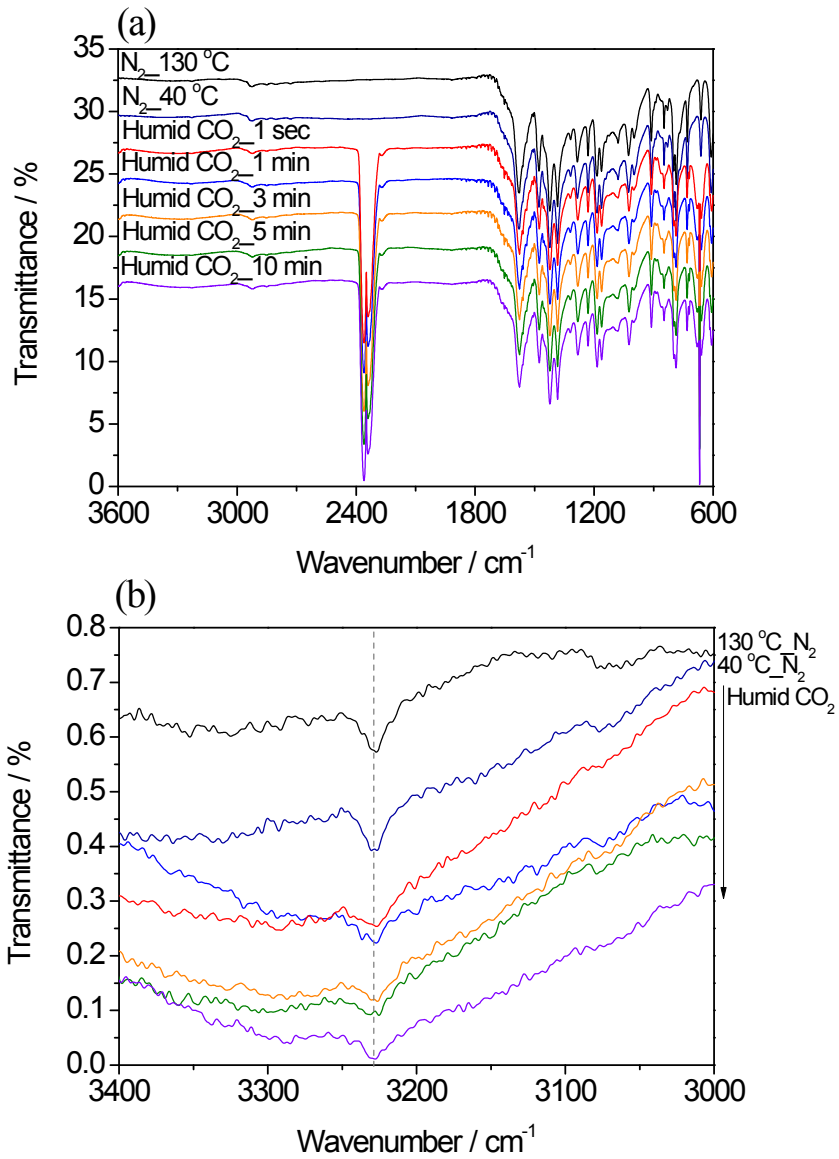

Fig. S20 (a) In-situ IR data of **1-ppz**. The cell was heated at 130 °C and then cooled down to 40 °C under N_2 flowing. Humid 15% CO_2 was infused into the cell and in-situ IR data were collected at different times. (b) Enlargement of the IR spectra in the high frequency range.

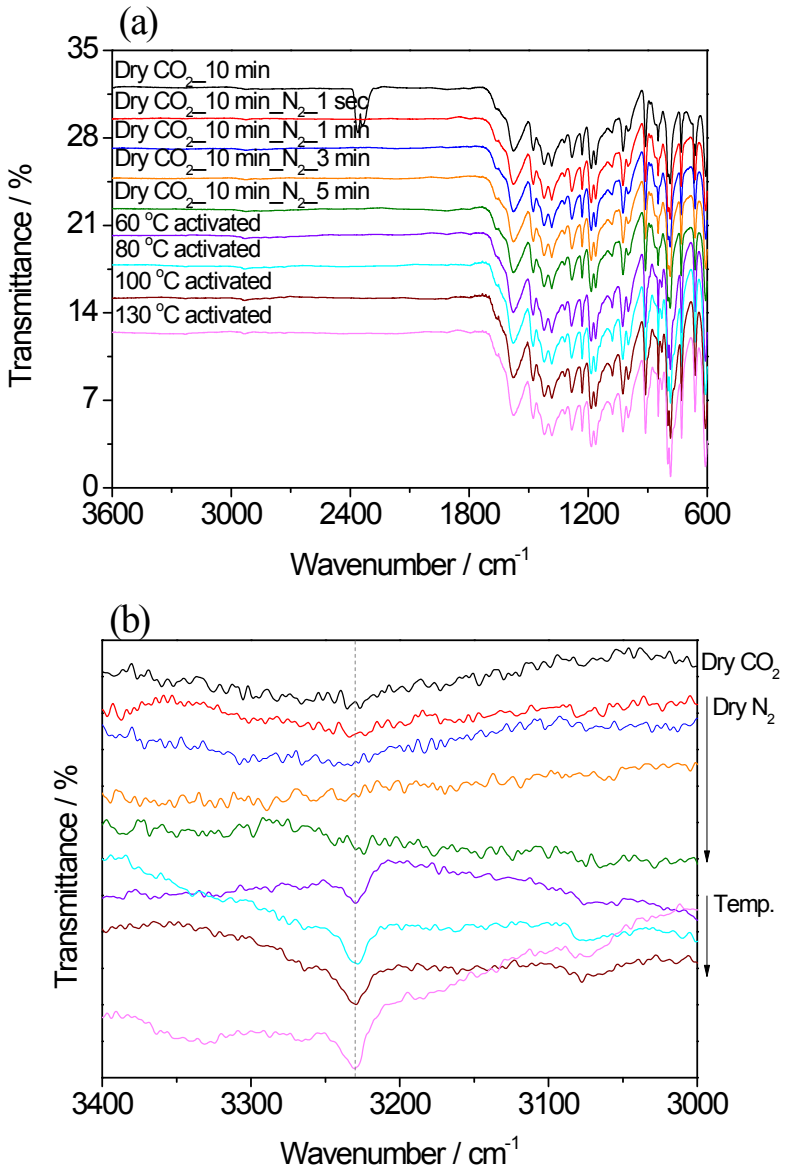

Fig. S21 (a) In-situ IR data of **1-ppz**. CO_2 (15%) was flowed into the cell for 10 min and then N_2 was infused into it for different times. The temperature was increased from 40 °C to 130 °C. (b) Enlargement of the IR spectra in the high frequency range.

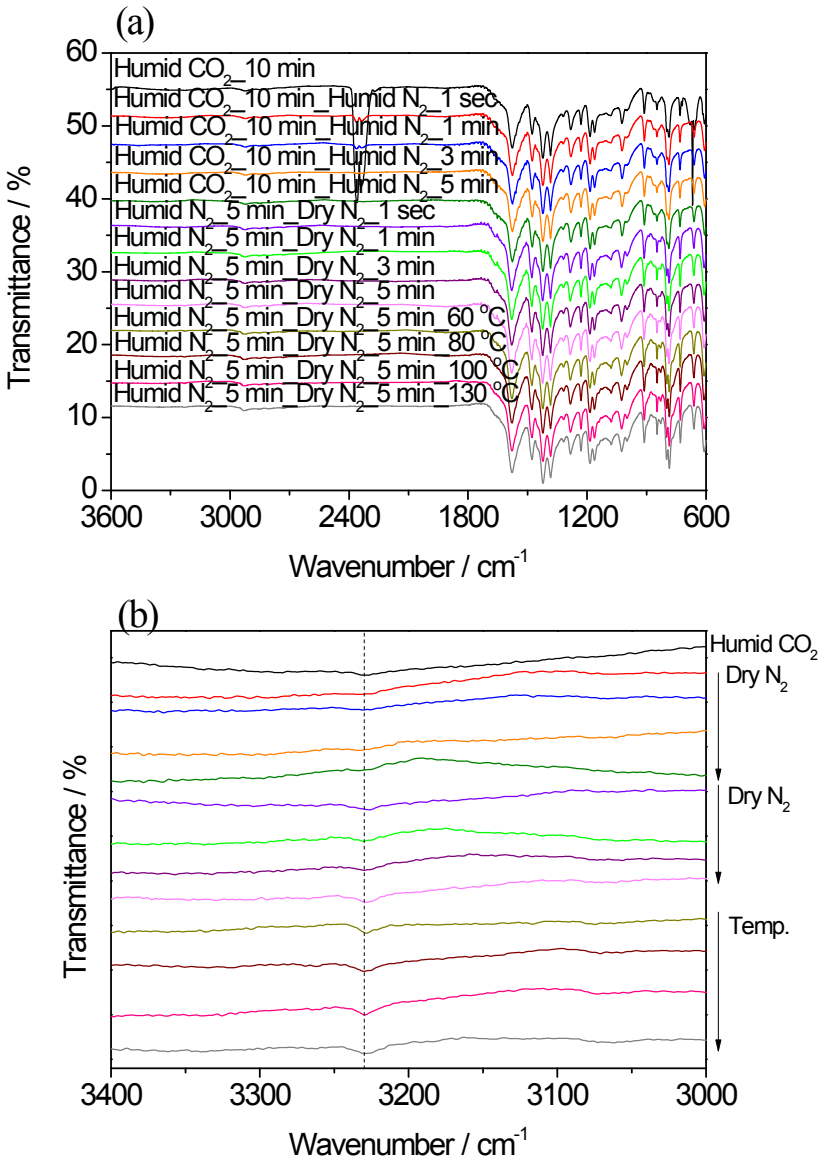

Fig. S22 (a) In-situ IR data of **1-ppz**. Humid CO_2 (15%) was flowed into the cell for 10 min and then N_2 was infused into it for different times. The temperature was increased from 40 ºC to 130 ºC. (b) Enlargement of the IR spectra in the high frequency range.

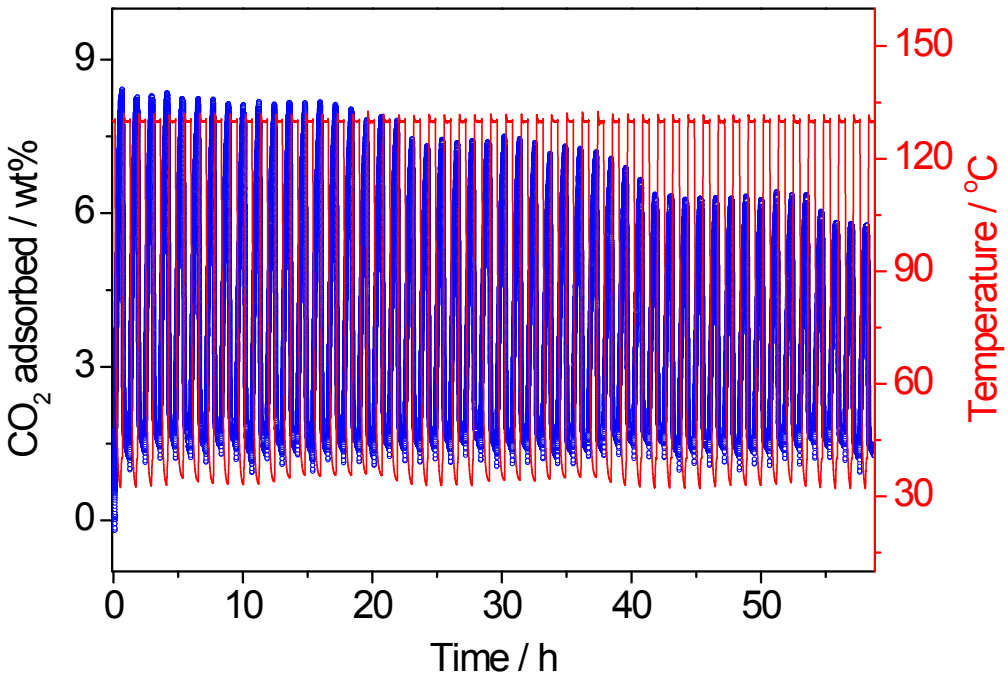

Fig. S23 TSA cycles of **1-ppz**. Adsorption at 15% CO_2 balanced with 85% N_2 and 40 °C for 30 min and desorption at Ar and 130 °C for 30 min were carried out.

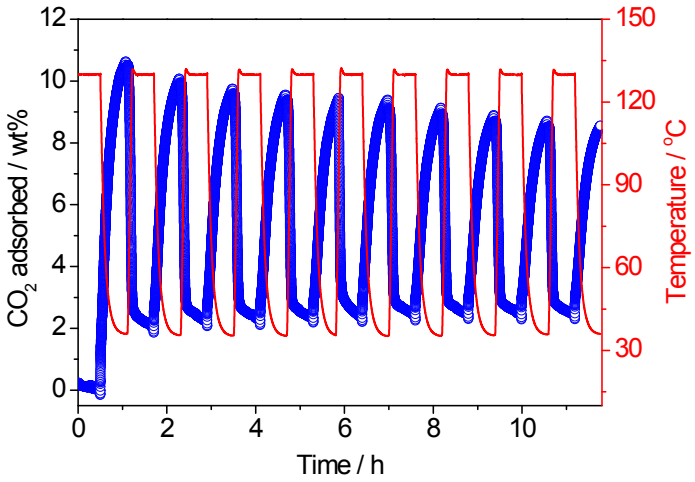

(a)

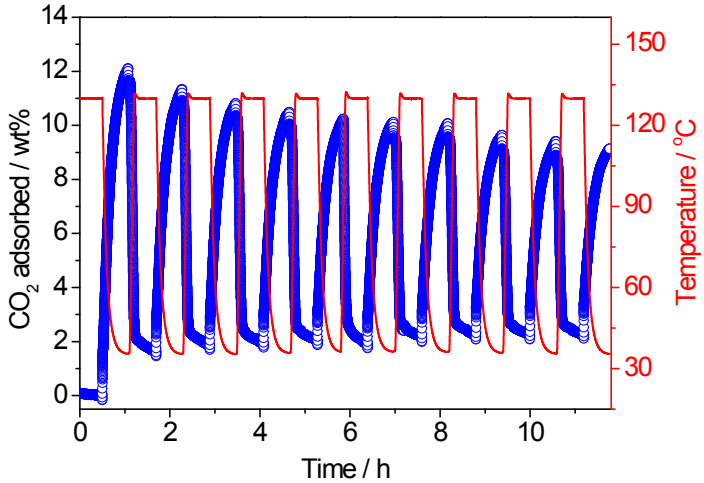

(b)

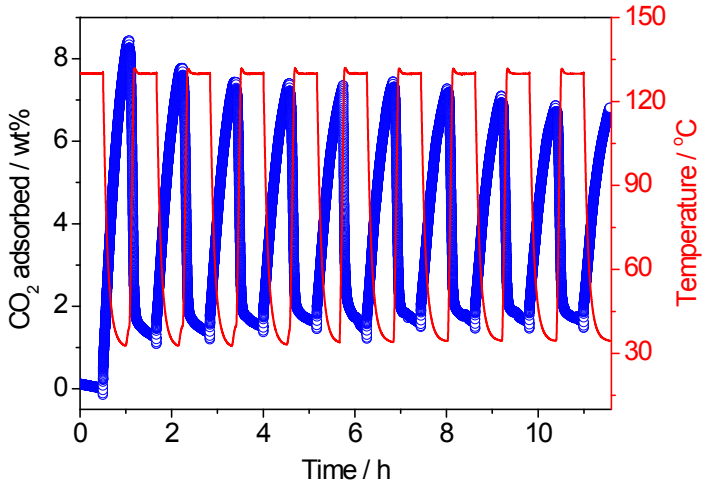

(c)

Fig. S24 TSA cycles of (a) **1-en**, (b) **1-mmen**, and **1-ppz**. Adsorption at 15% CO_2 balanced with 5% O_2 and 80% N_2, and 40 °C for 30 min and desorption at Ar and 130 °C for 30 min were carried out.

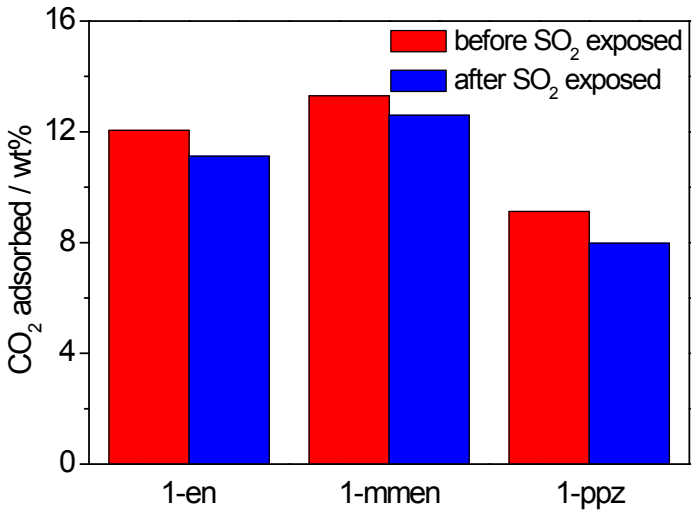

Fig. S25 CO_2 capacity before and after exposure to 500 ppm SO_2 balanced with N_2.

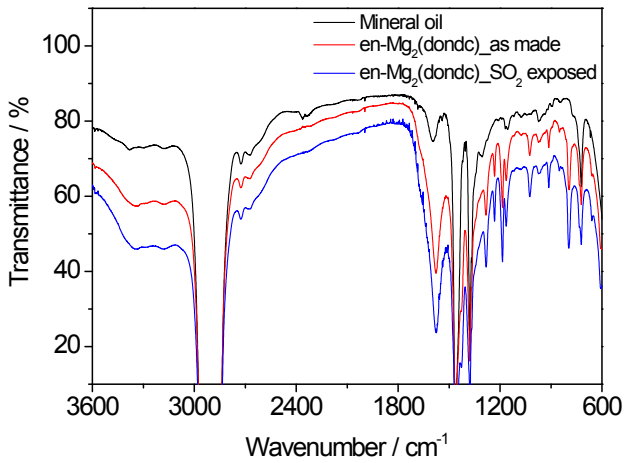

(a)

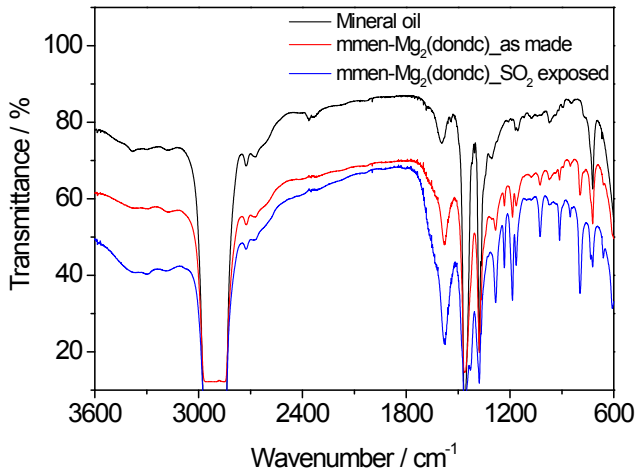

(b)

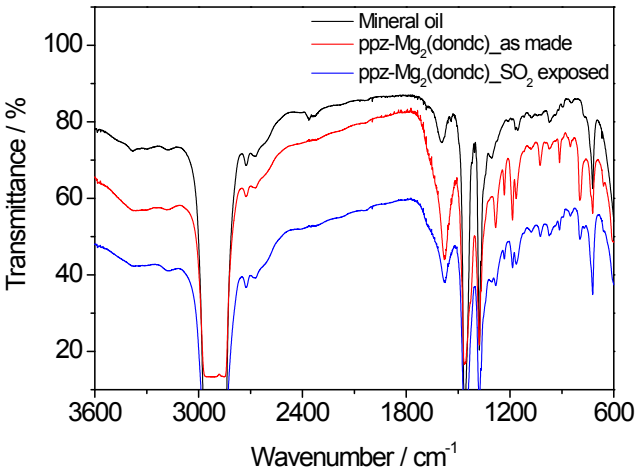

(c)

Fig. S26 Nujol IR data of (a) **1-en**, (b) **1-mmen**, and **1-ppz** before and after exposure to 500 ppm SO_2 in N_2.

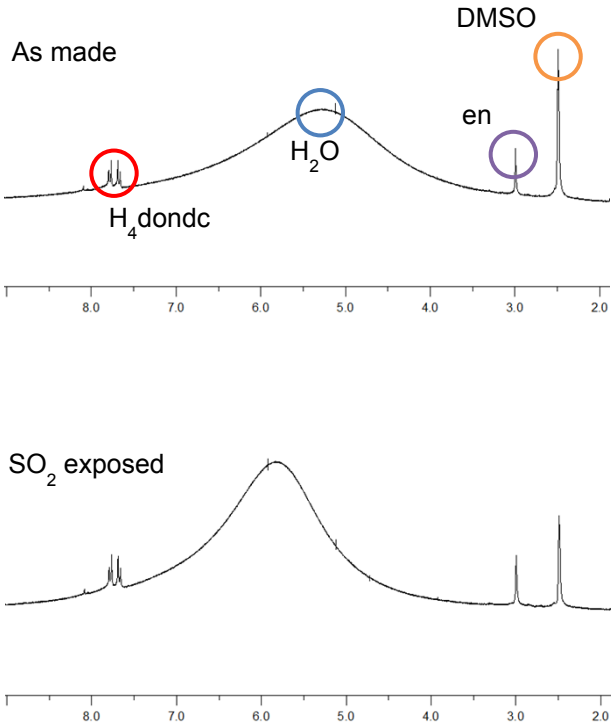
As made
DMSO
en
H_2O
H_4dondc
8.0
7.0
6.0
5.0
4.0
3.0
2.0
SO_2 exposed
8.0
7.0
6.0
5.0
4.0
3.0
2.0

(a)

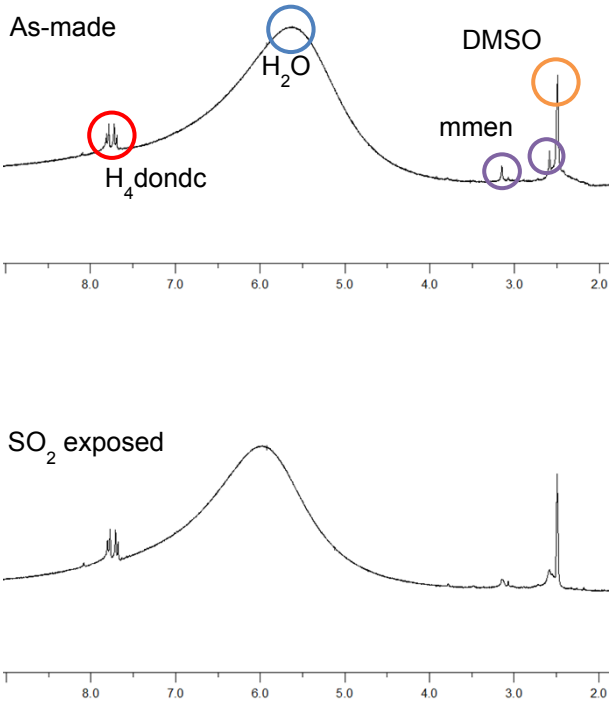
As-made
H_2O
DMSO
mmen
H_4dondc
8.0
7.0
6.0
5.0
4.0
3.0
2.0
SO_2 exposed
8.0
7.0
6.0
5.0
4.0
3.0
2.0

(b)

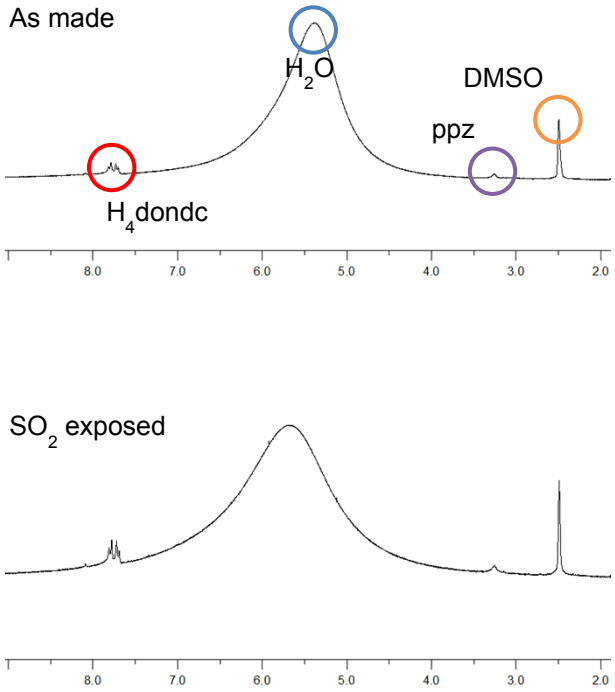

(c)

Fig. S27 NMR data of (a) **1-en**, (b) **1-mmen**, and **1-ppz** before and after exposure to 500 ppm SO_2 in N_2. Before the measurement, we digested each sample using DMSO-d_6 and 48% HF

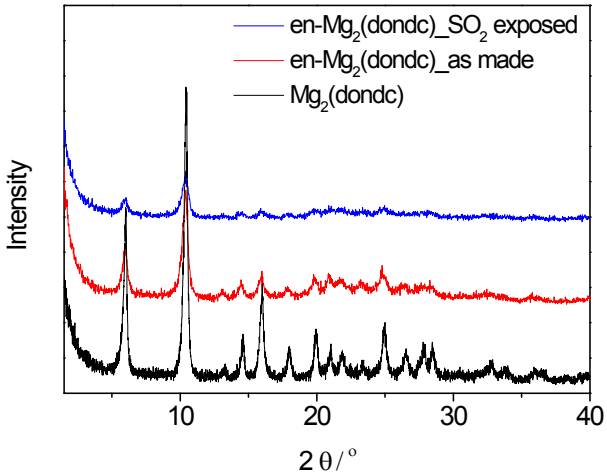

(a)

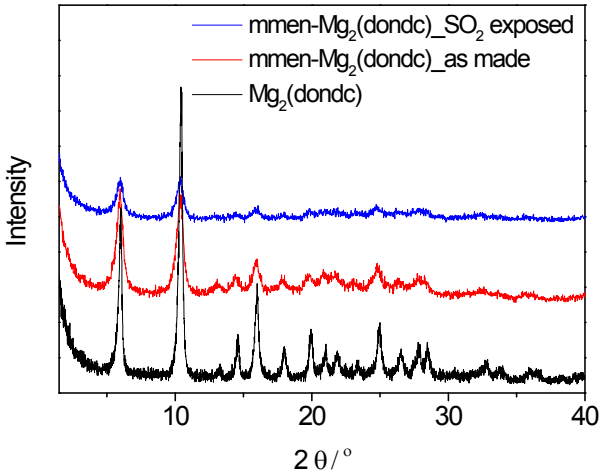

(b)

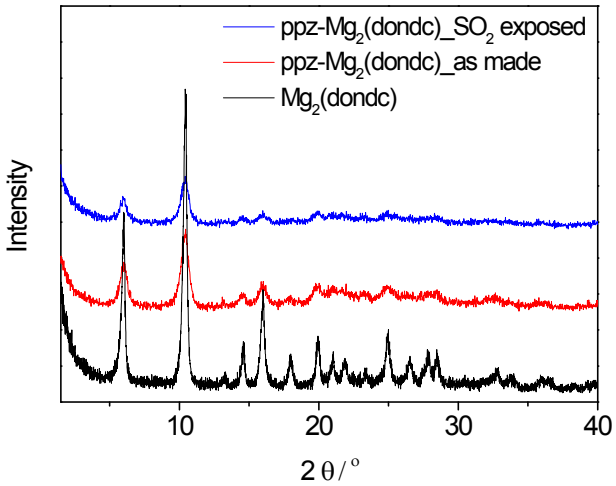

(c)

Fig. S28 PXRD data of (a) **1-en**, (b) **1-mmen**, and **1-ppz** before and after exposure to 500 ppm SO_2 in N_2

Table S6. Selectivity calculated from difference in breakthrough times of CO_2 and N_2.

N_2 breakthrough time (min/g)	3.2	3.2
CO_2 breakthrough time (min/g)	22	32
Breakthrough CO_2/N_2 selectivity	6.9	10